Maximum power extraction on wind turbine systems using block-backstepping with gradient dynamics control

Fernando Jaramillo-Lopez[1,*,†], Godpromesse Kenne[2] and Francoise Lamnabhi-Lagarrigue[1]

[1]*Laboratoire des Signaux et Systèmes, Supelec, Plateau du Moulon, 91192 Gif-sur-Yvette, France*
[2]*Laboratoire d'Automatique et d'Informatique Appliquée, Département de Genie Electrique, IUT-FV Bandjoun, Université de Dschang, Cameroun*

In this work, a novel adaptive control scheme that allows driving a stand-alone variable-speed wind turbine system to its maximum power point is presented. The scheme is based on the regulation of the optimal rotor speed point of the wind turbine. In order to compute the rotor speed reference, a model-based extremum-seeking algorithm is derived. The wind speed signal is necessary to calculate this reference, and a novel artificial neural network is derived to approximate this signal. The neural network does not need off-line learning stage, because a nonlinear dynamics for the weight vector is proposed. A block-backstepping controller is derived to stabilize and to drive the system to the optimal power point; to avoid singularities, the gradient dynamics technique is applied to this controller. Numerical simulations are carried out to show the performance of the controller and the estimator.

KEY WORDS: adaptive control; nonlinear systems; wind turbine systems; wind speed estimation; model-based extremum-seeking algorithms; renewable energy systems

1. INTRODUCTION

The compromising situation of the environment because of pollution and the high costs of the fossil fuels have originated new policies and regulations that have stimulated the interest on alternative energy sources. Many countries around the world have increased in an important way the penetration of these energy sources [1]. The wind energy conversion system is one of these systems. It converts wind energy into electricity by means of an electromechanical process.

In recent years, small wind turbines (1–100 kW) have been receiving attention as serious contributors for powering homes, farms, and small businesses. A class of small wind turbines are those using surface mount permanent magnets synchronous generators (PMSG) [2].

There exists two types of wind turbine systems (WTS): constant-speed turbine systems and variable-speed turbine systems (VST). Constant-speed turbine systems operate at fixed rotor speed and can be connected to the utility grid directly; VST operate at variable rotor speed and need power converter systems to convert the generated variable-frequency power to the fixed utility grid frequency. VST can work most of the time at maximum power point; also, they present lower loads. These facts have occasioned that they are preferred in the industry for utility-scale installations [3].

Depending on the wind speed, VST can operate in three regions, as it is shown in Figure 1. The region 1 is when the wind speed signal is under the cut-in wind speed v_{min}. A stopped turbine or

*Correspondence to: Fernando Jaramillo-Lopez, Département de Signaux, Laboratoire des Signaux et Systèmes, Supelec, Plateau du Moulon, 91192 Gif-sur-Yvette, France.
†E-mail: nandojalo@mail.com

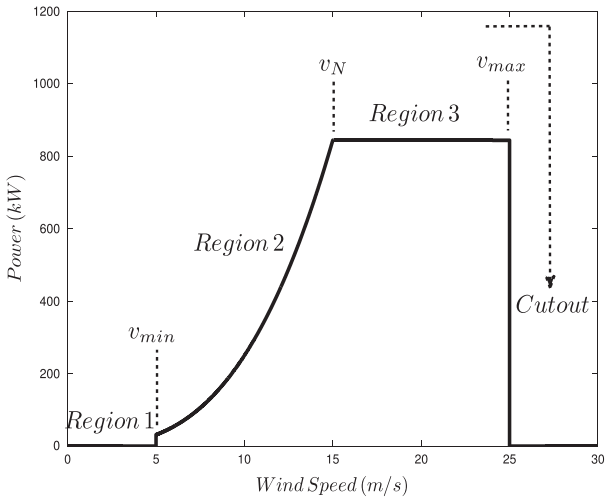

Figure 1. Operation regions for variable-speed turbine systems.

a turbine that is just starting up is considered to be operating in this region. No maximization of efficiency occurs on this region. Region 2 is when wind speed is above v_{min} but under the rated value v_N. In this region, the main controller task is to increase the efficiency of the WTS, operating it at its maximum power point (MPP). This is the main operational region. Region 3 is when wind speed is above v_N but under the cut-out wind speed v_{max}. In this region, the controller task is to keep the captured power at a fixed or rated value, instead of trying to maximize it. Another important controller task in this region is to keep the electrical and structural conditions in a safety region. This is done by varying the blade pitch. When the wind speed signal is above v_{max}, VST shut-down in order to preserve the system integrity.

In wind speed estimation-based control, the more usual way to achieve maximum power point tracking (MPPT) is by calculating the optimal rotor speed reference (ORSR) with the help of an optimal ratio value that is assumed to be known and the estimation of the wind speed; then the main problem turns into a regulation control problem. Several ways to estimate the wind speed have been reported. In [4], an interesting estimator for wind speed was proposed. It uses the immersion and invariance technique (I&I) to estimate the nonlinearly parametrized wind speed signal. It was shown that under some conditions based on the power coefficient function and the rotor speed, the estimator is asymptotically consistent. Artificial neural networks have been used in the identification of dynamic systems. See [5, 6] for discrete time systems and [7, 8] for continuous systems. In [8], the authors proposed a framework for time-varying parameter estimation in the continuous time-domain for a large class of nonlinear systems using a sliding-neural observer. In [9–11] and [12], the authors used artificial neural networks to estimate the wind speed directly; however, in those solutions, the node parameters (the weight vector included) need to be calculated off-line with an extensive set of input vectors. In some real-time conditions, the output of these estimators can be inaccurate, specially when these conditions were not included in the training input vectors. Also, in some operating points, the estimators can give wrong estimations of the wind speed signal [10]. In [13], the authors used the mechanical torque equation to estimate the wind speed. First, the mechanical torque is estimated using a Kalman filter, and then, the wind speed signal is calculated solving the mechanical torque equation for the wind speed using the Newton algorithm. The main drawback of this method is the iterative process in the Newton algorithm.

Perturbation-based and model-based extremum-seeking techniques have been used to solve many practical applications [14–17]. In [18], Guay *et al.* presented an adaptive extremum-seeking framework that is capable of driving the states of a nonlinear system to the desired set-points that maximize a given objective function. See that work for a detailed explanation of the model-based extremum-seeking technique. In that work, it is assumed that the structure of the objective function is known, but some parameters can be unknown. A controller is derived using the inverse optimal

design technique. The main drawbacks of that work are that the analysis is done considering constant parameters and a dither signal is added to the controller to help in the convergence of the estimates to their true values, but this excitation signal is also a perturbation that keeps away the states from their optimal values. In [14], the authors presented an application of the previous work, but this time, they assumed that part of the objective function is unknown and they used a neural network to approximate that part. They used the same technique, and the drawbacks are the same, but this result is interesting because part of the structure of the objective function can be considered unknown.

The model-based extremum-seeking technique is used in this paper to calculate the optimal rotor speed reference. In [19], the authors presented a similar extremum-seeking algorithm to derive the dynamics of an optimal reference; however, in that work, the analysis was made considering the dynamics of the plant as linear time-invariant, and the optimal value of the objective function as time invariant.

Many works have been focused on MPPT control of WTS. Some of them used linear techniques; however, the dynamics of the wind turbine systems have strong nonlinearities, and the wide range operation of these systems make that linear techniques are not well suited for this problem.

The main nonmodel-based control algorithms for MPPT control of WTS are the perturb and observe, hill-climb search, and the perturbation-based extremum-seeking algorithm. See [20–22] and [23] for a detailed explanation of some of these techniques. The main advantages of these algorithms are their simplicity and the fact that they do not need the model of the wind turbine system; however, the main drawback of these nonmodel-based control algorithms is that they work most of the time in a suboptimal operation point. For example, for the perturb and observe method, larger step-size means a faster response and more oscillations around the peak point, and hence, less efficiency; a smaller step-size improves efficiency but reduces the convergence speed [20]. This method also has the important inconvenience that the torque oscillations produced by the continuously changing operation point could damage the mechanical system, especially if its resonance frequency is excited [22].

Different authors have faced the MPPT problem neglecting the generator dynamics and using the electrical torque as an actual control variable; refer to [3] and [4]. Some works have been proposed that claim the achievement of certain control objectives like those in [24–26] and [27]; but theoretical stability analysis is not given. In [28], the authors proposed a sensorless robust control scheme of variable-speed wind turbine systems using the optimal torque control method. See the references therein for other related control works. Another sensorless control scheme for variable-speed wind turbine systems was proposed in [29]. In that work, a backstepping controller was derived and asymptotic stability was proved. In [2], the authors proposed a standard passivity-based controller (SPBC) that takes into account the generator dynamics and asymptotic stability of the equilibrium point was proved. This controller works well under slow variations in the wind input signal.

Some works have been proposed for fault detection and fault tolerant control of wind turbine systems. In [30] and [31], the authors presented two test benchmark models for the evaluation of fault detection and accommodation schemes for utility-scale wind turbine systems. The implementation of fault detection and supervisory control strategies for two 600-kW wind turbines at the National Renewable Energy Laboratory's National Wind Technology Center was described in [32]. In that work, the authors shared field experience obtained during the development and field testing of the existing fault detection system in both turbines. In [33], the author proposed three novel sensor fault detection and isolation algorithms for wind turbines with doubly fed induction generators.

In this paper, a novel algorithm to compute the ORSR, a new procedure to estimate the wind speed, and a novel block-backstepping controller with the gradient dynamics technique are presented and applied to the optimal control of wind turbine systems.

A model-based extremum-seeking algorithm is derived to compute the ORSR; it uses sliding mode theories to maximize the objective function. Uniform asymptotic stability of the error origin is proved using Lyapunov arguments. This is done considering that the optimum value in the objective function is time varying. This analysis is different from the one investigated in most previous works in extremum seeking that considers the optimum value in the objective function as time invariant.

The wind speed is calculated using the optimal mechanical torque value that is approximated with a neural network identifier. This neural identifier is derived based on the work proposed in [8]; however, no sliding techniques are used, and a nonlinear dynamics is proposed. This neural identifier is not used to estimate unknown parameters like in [8], neither to estimate the wind speed directly, but to approximate the unknown mechanical torque signal. The proposed neural network has a real-time dynamic nonlinear learning law (as opposed to off-line training procedure) of the weight vector. Uniform asymptotic stability of the error origin is proved using Lyapunov theories. The nonlinear learning law makes that the neural network can approximate very fast changing data. In this form, off-line training with extensive input data is not necessary. Also, good accuracy in any operation condition is guaranteed and continued learning is achieved.

A novel block-backstepping controller is derived to regulate the optimal equilibrium point; and the main contribution in this part of the adaptive scheme is that to avoid singularities the recent gradient dynamics technique proposed in [34] is applied. Uniform asymptotic stability of a small neighborhood of the tracking error origin for the overall system is proved using Lyapunov arguments, and the performance of this controller is compared with a classical PI controller and an SPBC that was proposed for the same system.

The paper is organized as follows. In Section 2, the mathematical model of the system is presented and the main problem is stated. The adaptive extremum-seeking algorithm that allows to calculate the optimal rotor speed reference is explained in Section 3. In Section 4, the procedure to calculate the wind speed is presented. The block-backstepping controller is derived in Section 5. In Section 6, numerical simulations for the block-backstepping controller, the PI controller, and the SPBC are presented and comparisons are made. Section 7 is devoted to conclusions and future research.

2. MATHEMATICAL MODEL AND PROBLEM STATEMENT

The system considered in this paper consists in a small-scale variable-speed wind turbine with a PMSG generator connected to a battery charging scheme. It is shown in Figure 2. The PMSG generator is connected to the battery system through a passive rectifier and a DC–DC converter.

The captured power by the wind turbine is given by

$$P_m = \frac{1}{2}\rho\pi r^2 C_p(\lambda) v_w^3 \tag{1}$$

where ρ is the density of the air, r is the rotor swept radius, $C_p(\lambda)$ is the power coefficient, and v_w is the wind speed. λ is the tip-speed ratio (TSR) and is given by the following expression:

$$\lambda \triangleq \frac{r\omega_m}{v_w},$$

where ω_m is the rotor speed.

The power coefficient data is obtained by experimental measurements or by using blade-element moment theory, and it depends on the size and geometry of the blades. Some works have been

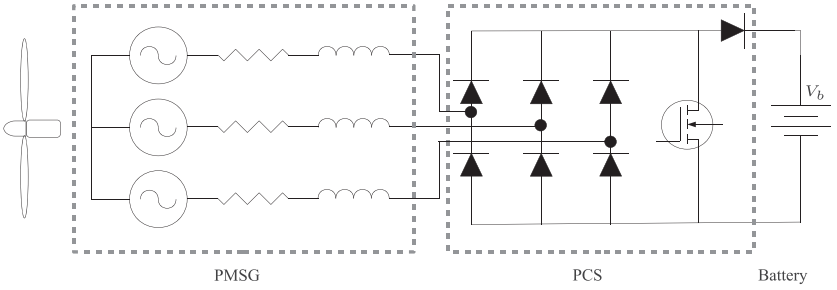

Figure 2. Wind turbine with surface mount permanent magnets synchronous generators generator.

proposed to characterize the $C_p(\lambda)$ expression, like the work presented in [35]. Although the general characterization of C_p depends not only on λ but also on the blade pitch θ, the present work aims to increase the efficiency of WTS in region 2, and θ will be considered as fixed, that is, $\theta \equiv 0$. The following characterization, taken from [36], is used in this work.

$$C_p(\lambda) = e^{-\frac{c_{p1}}{\lambda}} \left(\frac{c_{p2}}{\lambda} - c_{p3} \right) + c_{p4}\lambda \tag{2}$$

where $c_{p1} = 21$, $c_{p2} = 125.2165$, $c_{p3} = 9.7798$, and $c_{p4} = 0.0068$.

The model of the PMSG generator in the dq framework is given by ([37], [38])

$$\begin{aligned} L\dot{i}_d &= -Ri_d + Li_q\omega_e - v_d, \\ L\dot{i}_q &= -Ri_q - Li_d\omega_e + \phi\omega_e - v_q \end{aligned}$$

where i_d and i_q are the dq currents; v_d and v_q are the dq voltages; R and L are the stator resistance and inductance, respectively; ϕ is the permanent magnetic flux; and the electric frequency ω_e is given by

$$\omega_e = \frac{P}{2}\omega_m,$$

with P the number of pole pairs.

Because of the topology used, the PMSG current has unity power factor and the dq voltages are determined by the battery voltage v_b and the duty ratio of the DC–DC converter D [2]:

$$\begin{aligned} v_d &= \frac{i_d}{\sqrt{i_d^2 + i_q^2}} k_{de} v_b D \\ v_q &= \frac{i_q}{\sqrt{i_d^2 + i_q^2}} k_{de} v_b D \end{aligned}$$

where $k_{de} = \frac{\pi}{3\sqrt{3}}$ is the diode gain.

The rotor speed dynamics is given by

$$\dot{\omega}_m = \frac{1}{J}T_m - \frac{1}{J}T_e$$

where J is the rotor inertia; T_m is the mechanical torque and T_e is the electrical torque:

$$T_e = \frac{3P}{4}\phi i_q.$$

The mechanical torque is given by the ratio between the captured power and the rotor speed:

$$T_m = \frac{P_m}{\omega_m} = \frac{1}{2}\rho\pi r^3 \frac{C_p(\lambda)}{\lambda} v_w^2. \tag{3}$$

The states of the system are defined by a scaling in the dq currents and the rotor speed:

$$x \triangleq \left[s_1 L i_d,\ s_2 L i_q,\ s_3 \frac{2J}{3r}\omega_m \right]^T$$

where $s_i > 0, i = 1, 2, 3$ is an additional scaling factor that helps to increase the region of attraction of the equilibrium point.

The model of the overall system is given by

$$\dot{x} = f(x, v_w) + G(x)u \tag{4}$$

where

$$f(x, v_w) \triangleq [f_1,\ f_2,\ f_3]^T\,, \quad G(x) \triangleq [g_1,\ g_2,\ 0]^T \tag{5}$$

and

$$f_1 = -\frac{Rx_1}{L} + \frac{3PLrs_1x_2x_3}{4LJs_2s_3} \tag{6}$$

$$f_2 = -\frac{Rx_2}{L} - \frac{3PLrs_2x_1x_3}{4LJs_1s_3} + \frac{3P\phi rs_2x_3}{4Js_3} \tag{7}$$

$$f_3 = T_{sm}(x_3, v_w) - g_{3v}x_2 \tag{8}$$

$$g_1 = -\frac{k_{de}v_bx_1}{L} \tag{9}$$

$$g_2 = -\frac{k_{de}v_bx_2}{L} \tag{10}$$

$$g_{3v} = \frac{P\phi s_3}{2Lrs_2} \tag{11}$$

with the control signal and the *scaled* mechanical torque, respectively:

$$u \triangleq \frac{D}{\sqrt{\left(\frac{x_1}{Ls_1}\right)^2 + \left(\frac{x_2}{Ls_2}\right)^2}}$$

$$T_{sm}(x_3, v_w) = \frac{2\rho\pi Js_3^2v_w^3}{9x_3}C_p\left(\frac{3r^2x_3}{2Js_3v_w}\right). \tag{12}$$

It is assumed that the states $x \in \mathbb{R}^3$ are measured; the model parameters are well known; the wind speed v_w is unknown, and the system is working in region 2, that is, $x_3 > 0$.

2.1. Equilibria and control objective

The main control objective is to regulate the rotor speed to its optimal value and to achieve, in this way, maximum power extraction. In wind speed estimation-based control (sometimes called TSR control), the more usual way to calculate the reference for the rotor speed is by using the estimated wind speed and the optimal TSR. In this work, a different approach is presented. This reference is calculated using an adaptive extremum-seeking algorithm —which is explained in the next section—

$$\hat{\hat{x}}_{3*}(\nabla_\lambda C_p).$$

The second reference of the equilibria is derived solving (8) for x_2:

$$x_{2*} = \frac{4\rho\pi LJrs_2s_3v_w^3}{9P\phi x_{3*}}C_p\left(\frac{3r^2x_{3*}}{2Js_3v_w}\right).$$

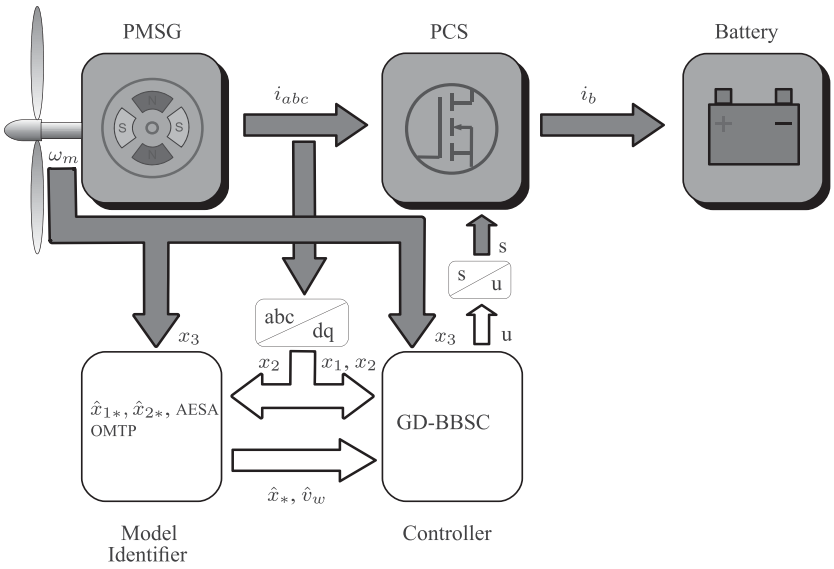

Figure 3. Block diagram of the wind turbine system.

The first reference for the two equilibrium points is given by solving (6) and (7) for x_1:

$$x_{1*} = \frac{\phi s_1}{2} \pm \frac{1}{2}\sqrt{(\phi s_1)^2 - \frac{4s_1^2 x_{2*}^2}{s_2^2}}.$$

The second equilibrium point (minus sign) will be used to drive the system to the optimal rotor speed operation point.

2.2. Block diagram

Figure 3 shows the block diagram of the overall wind turbine system. The gray blocks represent the physical components, whereas the white blocks represent the algorithms. The gray arrows represent the physical signals, whereas the white arrows represent the information flow between the algorithms. The model identifier block is composed by the wind speed estimator based in the optimal mechanical torque point, which is explained in Section 4, and the adaptive extremum-seeking algorithm, which is used to calculate the reference signal for the third state, and is explained in the next section. This block also calculates the reference signals for the first and second states. This information, the estimated wind speed signal, and the three signal references, along with the three measured states, feed the gradient dynamics-block-backstepping controller (GD-BBSC).

3. ROTOR SPEED REFERENCE CALCULATION

In this Section, the model-based extremum-seeking algorithm that allows to calculate the rotor speed reference is derived as follows.

The objective function is given by the power coefficient function

$$y \triangleq C_p(\lambda_f) \tag{13}$$

with

$$\lambda_f = \frac{3r^2 x_3}{2Js_3 v_{w_f}}$$

and

$$v_{w_f} \triangleq \frac{1}{\tau s + 1} v_w$$

where the wind speed signal in the argument of C_p is filtered. The low-pass filter is added to eliminate high-frequency components of the wind speed signal caused by wind gusts, as these components can be reflected in the control signal causing unnecessary stress on the structure. This filter is incorporated in the wind speed estimator.

Using the power coefficient (2) given in Section 2, and computing its gradient, yields

$$h \triangleq \frac{\partial y}{\partial \lambda_f} = \frac{1}{\lambda_f^2} e^{-\frac{c_{p1}}{\lambda_f}} \left(\frac{c_{p1} c_{p2}}{\lambda_f} - c_{p2} - c_{p1} c_{p3} \right) + c_{p4}.$$

In order to calculate the rotor speed reference, we need to maximize the power coefficient function C_p; this can be done by vanishing its gradient h. The following assumption is necessary to derive the algorithm.

Assumption 1
There exists a unique λ_* maximizing the objective function (13) on the compact set Ω_y, that is,

$$\left. \frac{\partial y(\lambda_f)}{\partial \lambda_f} \right|_{\lambda_f = \lambda_*} = 0, \qquad \left. \frac{\partial^2 y(\lambda_f)}{\partial \lambda_f^2} \right|_{\lambda_f = \lambda_*} < 0 \quad \forall\ \lambda_* \in \Omega_y$$

$$\left. \frac{\partial y(\lambda_f)}{\partial \lambda_f} \right|_{\lambda_f = \lambda_* + \epsilon} \epsilon < 0 \quad \forall\ (\lambda_* + \epsilon) \in \Omega_y.$$

Remark 1
This assumption means that the objective function is strictly convex on a certain interval. The power coefficient function, in general, always satisfies this assumption, at least for a subset in its domain. For the power coefficient function given by (2), it is satisfied for all its domain.

Because the wind speed signal in λ_f is unknown, the following algorithm is proposed to bring the rotor speed reference to the optimal trajectory:

$$\dot{\hat{x}}_{3*} \triangleq \begin{cases} k_{g1} \text{sign} \hat{h} & \text{if} \quad |\hat{h}| \leqslant \epsilon_{x_{3*}} \\ k_{g2} \text{sign} \hat{h} & \text{otherwise} \end{cases} \tag{14}$$

where

$$\hat{h} \triangleq \left. \frac{\partial y}{\partial \lambda_f} \right|_{\lambda_f = \hat{\lambda}}$$

$k_{gi} > 0; i = 1, 2.\ \epsilon_{x_{3*}} \geqslant 0$; and

$$\hat{\lambda} = \frac{3 r^2 x_3}{2 J s_3 \hat{v}_w}$$

with $\hat{v}_w$ the estimated wind speed, which is derived in the next section.

Two gains (k_{gi}) are introduced in the present scheme to reduce the chattering problem. The bigger one is used when the estimated reference is far from its optimal point and the smaller one when the

estimated reference is in the neighborhood of the optimal point. In order to prove stability of the estimated reference, consider the following definition and assumption.

$$\tilde{x}_{3*} = x_{3*} - \hat{\tilde{x}}_{3*}$$

where x_{3*} is the time-varying ideal reference for the third state, which is assumed to be unknown, and $\hat{\tilde{x}}_{3*}$ is the estimated reference.

Assumption 2
The derivative of the ideal third reference x_{3*} is bounded by a known value:

$$\|\dot{x}_{3*}\| \leqslant \mu_{x_{3*}}$$

where $\mu_{x_{3*}}$ is a known positive number.

If the sliding mode gains are chosen in this way:

$$k_{gi} > \mu_{x_{3*}}, \qquad i = 1, 2 \tag{15}$$

then, the following results.

Lemma 1
Consider the reference given by (14) satisfying assumptions 1, 2 and condition (15), then the origin of the $\tilde{x}_{3*}$ error is uniformly asymptotically stable.

Proof
As it is shown in the next Section, the wind speed estimation error depends on the neural identifier error e and the tracking error of the third state $\tilde{x}_3$: $\hat{v}_w(e, \tilde{x}_3)$. Considering this fact, the estimated gradient can be defined as

$$\sigma = h(\lambda_f) - e_h(e, \tilde{x}_3) \tag{16}$$

where $e_h(e, \tilde{x}_3) = h(\lambda_f) - \hat{h}(\hat{\lambda})$ is the gradient error.

Let us define the perturbation set, and its complement, for the estimated reference of the wind turbine system

$$\Omega_\epsilon = \left\{\sigma : \left|h(\lambda_f)\right| \leqslant \epsilon\right\}$$
$$\bar{\Omega}_\epsilon = \left\{\sigma : \left|h(\lambda_f)\right| > \epsilon\right\}$$

where

$$\epsilon = |e_h(e, \tilde{x}_3)|$$

is the size of the perturbation. For all $\sigma \in \bar{\Omega}_\epsilon$ (outside of the perturbation region), $\tilde{x}_{3*}$ and the function sign(σ) have the same signs (Figure 4).

To prove convergence to the sliding surface, consider the following Lyapunov candidate function

$$V = \frac{1}{2}\tilde{x}_{3*}^2$$

its time derivative is

$$\begin{aligned}\dot{V} = \tilde{x}_{3*}\dot{\tilde{x}}_{3*} &= -\tilde{x}_{3*}\left[k_{gi}\text{sign}\sigma - \dot{x}_{3*}\right] \\ &\leqslant -|\tilde{x}_{3*}|\left(k_{gi} - \mu_{x_{3*}}\right) \qquad \forall\ \sigma \in \bar{\Omega}_\epsilon.\end{aligned}$$

Because $\dot{V}$ is negative on the boundary of Ω_ϵ, then the set Ω_ϵ is positively invariant. This results in a sliding mode regime on $\sigma = 0$ in finite time. Considering this fact, and (16), it results

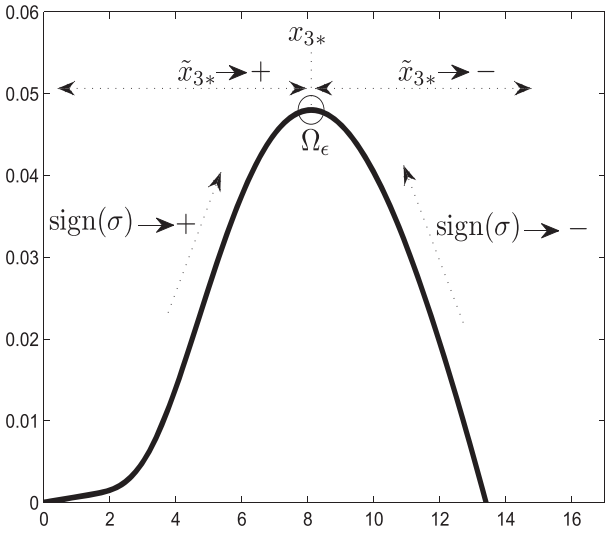

Figure 4. Coefficient power function C_p and third reference variables.

$$h(\lambda_f) = e_h(e, \tilde{x}_3)$$

where the right side of this equation is the size of the perturbation neighborhood around the optimal point. In Section 4, it is established that the neural identifier error vanishes asymptotically; also in Section 5, it is shown that the tracking error $\tilde{x}_3$ vanishes in the same way; therefore, it yields

$$\lim_{t\to\infty} e_h(e, \tilde{x}_3) = 0$$

and

$$\lim_{t\to\infty} \hat{h}(e, \tilde{x}_3) = h$$

which means that the power coefficient gradient will reduce until enter in the perturbation region in finite time, and then it will vanish asymptotically. □

Remark 2
It seems that the assumption about the known $\mu_{x_{3*}}$ bound is too strong; in addition, we need this bound to set the adaptive gains k_{gi} to a bigger value. To explain the significance of this assumption, first, we need to recall that the physical nature of wind makes that the bound on $\|\dot{x}_{3*}\|$ exists; second, this bound can be very high —because of strong gusts—; however, we are not interested on track these high-frequency components of the wind; therefore, the $\mu_{x_{3*}}$ bound is not a need for the knowledge of the maximal value of $\|\dot{x}_{3*}\|$, but it is a threshold value of $\|\dot{x}_{3*}\|$ under which convergence is achieved as the preceding analysis has demonstrated it. In other words, when the magnitude of the derivative of x_{3*} is smaller than k_{gi}, then, convergence is guaranteed; so we need to set the k_{gi} gains properly, to cover the desired wind spectrum, but not too high, because this will increase the chattering problem.

4. WIND SPEED CALCULATION

In this section, the procedure to calculate the wind speed signal is described. The wind speed can be estimated using the mechanical power (1) or the mechanical torque (3). With the knowledge of the mechanical torque value, the wind speed can be calculated solving the mechanical torque equation

for v_w. In this paper, instead of solving the equation on-line with an iterative algorithm, the scaled mechanical torque (12) evaluated at its optimal point

$$T_{sm*}(x_{3*}, v_w) = \frac{s_3 \rho \pi r^2 C_{p*} v_w^2}{3\lambda_*}$$

—where $C_{p*} = C_p(x_{3*}, v_w)$ and λ_* are well known values— is used to solve the wind speed with a direct relationship

$$\hat{v}_w = \frac{1}{\tau s + 1} \sqrt{\frac{3\hat{T}_s \lambda_*}{s_3 \rho \pi r^2 C_{p*}}}$$

where τ is the time constant of the low-pass filter and s is the Laplace variable;

$$\hat{T}_s \triangleq \begin{cases} \hat{T}_{sm}(t, x_3, \hat{x}_3, \hat{w}) & \text{if} \quad \hat{T}_{sm}(\cdot) \geqslant 0 \\ 0 & \text{otherwise} \end{cases}$$

$\hat{T}_{sm}(t, x_3, \hat{x}_3, \hat{w})$ is the approximation of the scaled mechanical torque given by the neural network identifier, and its definition is given in (18).

This approach presents two inconveniences:

1. The system needs to operate at its optimal mechanical torque/rotor speed point,
2. The mechanical torque needs to be measured or estimated.

But the first point is also the main control objective of this system, so it results in the derivation of a good controller that is able to satisfy this objective. In Section 5, this controller is presented, and uniform asymptotic stability of a small neighborhood of the tracking error origin is proved. In Section 6, the numerical simulations show the good performance of this controller and the validity of this wind speed calculation.

For the second point, a neural network identifier is proposed to estimate the scaled mechanical torque T_{sm}. This signal can be expressed as follows

$$T_{sm}(t, x_3) = T_{smn}(x_3) + \delta(t)$$

where $T_{smn}(x_3)$ is the nominal value of the signal T_{sm}, which is continuous and bounded on a compact set Ω_n; $\delta(t)$ is the uncertain part of the signal because of changes in the wind speed, and it is assumed to be bounded too. The nominal part of this signal is continuous and can be approximated by a radial basis function neural network (RBFNN) [5, 6]. Thus, the scaled mechanical torque can be described as follows [8]

$$T_{sm}(t, x_3) = \Psi(x_3, w^*) + e_f(x_3) + \delta(t)$$

with

$$\Psi(x_3, w^*) = \sum_{j=1}^{N} w_j^* \phi_T(||x_3 - C_j||, v) \tag{17}$$

where $\phi_T(\cdot)$ denotes a nonlinear function; C_j and v, $j = 1, \ldots, N$ are the center and the width of the jth hidden unit, respectively; N is the number of the hidden nodes or RBFNN units; w^* is the optimal weight vector that satisfies $||w^*|| \leqslant R_w$, with R_w a positive constant; x_3 is the input of the RBFNN; $e_f(x_3)$ is the optimal approximation error, which is unknown and bounded $\forall x_3 \in \Omega_n$.

Proportional error terms are introduced to improve the convergence of the neural network in the presence of the uncertainty δ. The function $T_{sm}(t, x_3)$ is approximated assuming that the terms δ and e_f are bounded by an unknown positive constant.

The following identifier is proposed to approximate the T_{sm} signal,

$$\dot{\hat{x}}_3 = \hat{T}_{sm}(t, x_3, \hat{x}_3, \hat{w}) - g_{3v}x_2 \tag{18}$$

with

$$\hat{T}_{sm}(t, x_3, \hat{x}_3, \hat{w}) \triangleq b(t, x_3, \hat{x}_3) + \Psi(x_3, \hat{w}).$$

The nonlinear function $\phi_T(\cdot)$ in (17) is the gaussian function and has the following form

$$\phi_T(x_3, v, C) = \exp\left[\frac{-||x_3 - C_j||^2}{v^2}\right]$$

the centers C_j and the width v of the jth hidden unit are chosen as follows

$$v = \frac{x_{3_{max}} - x_{3_{min}}}{N}$$
$$C_j = x_{3_{min}} + \frac{2j-1}{2}v$$

where $x_{3_{\min}}$ and $x_{3_{\max}}$ are the lower and upper bounds of the RBFNN input x_3, respectively.

In order to get asymptotic convergence of the neural identifier, let the term $b(t, x_3, \hat{x}_3)$, the learning rule of the weight vector $\hat{w}$, and the adaptive law $\hat{\lambda}_T$ be chosen as follows

$$b(t, x_3, \hat{x}_3) = -\hat{\lambda}_T e \tag{19}$$

with

$$\dot{\hat{\lambda}}_T = \begin{cases} -k_{\lambda_T}\hat{\lambda}_T & \text{if} \quad e = 0 \\ \alpha & \text{otherwise} \end{cases} \tag{20}$$

where $e = \hat{x}_3 - x_3$, k_{λ_T} and $\alpha > 0$,

$$\begin{aligned} \dot{\hat{w}}_j &= \text{Proj}\left[-(k_w e)^3 \frac{\partial \Psi}{\partial w_j}\bigg|_{w_j = \hat{w}_j}\right] \\ &= \begin{cases} -(k_w e)^3 \frac{\partial \Psi}{\partial w_j}\Big|_{w_j = \hat{w}_j} & \text{if} \quad |\hat{w}_j| \leqslant R_w \\ 0 & \text{otherwise} \end{cases} \end{aligned} \tag{21}$$

with $k_w > 0$ and Proj$(\cdot)$ the projection function on the compact set $\Omega_w = \{w : ||w|| \leqslant R_w\}$, it guarantees that the estimates $\hat{w}_j$ remain bounded.

The dynamics of the neural identifier error e is given by

$$\dot{e} = \Psi(x_3, \hat{w}) - \Psi(x_3, w^*) + b(t, x_3, \hat{x}_3) - e_f(x_3) - \delta(t).$$

Using Taylor series expansion and the fact that the neural network is a linear function of $\hat{w}$, the last equation can be rewritten as

$$\dot{e} = b(t, x_3, \hat{x}_3) + \sum_{j=1}^{N} \frac{\partial \Psi}{\partial w_j}\Big|_{w=\hat{w}_j} \tilde{w}_j - e_f(x_3) - \delta(t)$$

where $\tilde{w}_j = \hat{w}_j - w_j^*$.

Now, let us consider the following assumptions.

Assumption 3
The optimal approximation error and the uncertainty in the T_{sm} signal are bounded, that is,

$$|e_f(x_3) + \delta(t)| \leqslant \lambda_T \tag{22}$$

where λ_T is an unknown positive constant.

Remark 3
The optimal approximation error of the neural network is bounded [5, 6], and the uncertainty in the T_{sm} signal is bounded because of its physical nature.

Assumption 4
All the trajectories $x(t)$ of the system (4) belong to a compact set Ω_x; the trajectories $\hat{x}_3(t)$ of the neural network identifier belong to a compact set $\Omega_{\hat{x}}$; the control signal u is such that $(x(t), \hat{x}_3(t))$ exist for all $t \geqslant 0$.

Remark 4
In Section 5, a block-backstepping controller is derived such that the aforementioned conditions on $x(t)$ are satisfied. The proof that $\hat{x}_3(t)$ is bounded is shown subsequently.

Lemma 2
Consider the system given by (4) and the neural network identifier (18), with the term $b(t, x_3, \hat{x}_3)$, the adaptive law of the unknown bound $\hat{\lambda}_T$ and the learning rule of the weights $\hat{w}_j$ given by (19), (20), and (21), respectively; satisfying Assumptions 3 and 4; and for all $(x(0), \hat{x}_3(0)) \in \Omega_x \times \Omega_{\hat{x}}$, then the neural identifier error e converges to the origin uniformly asymptotically.

Proof
Let us propose the following Lyapunov function candidate

$$V_o(e, \tilde{w}) = \frac{1}{4}e^4 + \frac{1}{2k_w^3}\sum_{j=1}^{N}\tilde{w}_j^2.$$

Its time derivative is

$$\begin{aligned}\dot{V}_o &= e^3\dot{e} + \frac{1}{k_w^3}\sum_{j=1}^{N}\dot{\hat{w}}_j\tilde{w}_j \\ &= e^3 b(t, x_3, \hat{x}_3) - e^3[e_f(x_3) + \delta(t)] \\ &\quad + \sum_{j=1}^{N}\tilde{w}_j\left(\frac{\dot{\hat{w}}_j}{k_w^3} + e^3\frac{\partial\Psi}{\partial w_j}\bigg|_{w=\hat{w}_j}\right).\end{aligned}$$

Considering (19), (21), and (22) yields

$$\dot{V}_o \leqslant -\hat{\lambda}_T e^4 + \lambda_T|e^3|. \tag{23}$$

This can be rewritten as

$$e^3\dot{e} \leqslant -\hat{\lambda}_T e^4 + \lambda_T|e^3| + \frac{1}{k_w^3}\sum_{j=1}^{N}\left|\dot{\hat{w}}_j\tilde{w}_j\right|.$$

From (20), it is clear that

$$\hat{\lambda}_T(t) = \alpha t + \hat{\lambda}_T(0) \quad \text{if} \quad e \neq 0$$

thus, the adaptive gains $\hat{\lambda}_T$ will always increase while the error e is not null. Also, the estimates $\hat{w}_j$ are bounded by construction; therefore, the following inequality holds

$$\lim_{t\to\infty} \hat{\lambda}_T e^4 > \lambda_T |e^3| + \frac{1}{k_w^3} \sum_{j=1}^{N} \left| \dot{\hat{w}}_j \tilde{w}_j \right|$$

and the identifier error e will converge uniformly asymptotically to the origin. □

5. CONTROLLER

In this section, a controller is derived for the analyzed plant. From (4)–(11), it is clear that the control signal does not drive the third state directly. Backstepping technique [39] seems to be a natural choice for this problem, using the second state x_2 as the virtual control input for the dynamics of x_3.

The following assumption is necessary to derive the block-backstepping controller.

Assumption 5
The wind speed signal v_w vary slowly such that its time derivative can be negligible with respect to other existing dynamics.

Remark 5
This assumption is to keep a simpler controller as it implies that the references are constants too.

The third state dynamics is controlled using x_2 as virtual control:

$$\dot{x}_3 = T_{sm}(x_3, v_w) - g_{3v} x_{2u},$$

x_{2u} is proposed as follows

$$x_{2u} \triangleq g_{3v}^{-1} \left[T_{sm}\left(x_3, \hat{v}_w\right) + \left(k_3 + \hat{\xi}_3\right) \tilde{x}_3 \right]$$

with $k_3 > 0$, $\tilde{x} = x - x_*$ and

$$\dot{\hat{\xi}}_i \triangleq \begin{cases} -k_{\xi_i} \hat{\xi}_i & \text{if} \quad e = 0 \\ \alpha_i & \text{otherwise} \end{cases}$$

where k_{ξ_i} and $\alpha_i > 0$; $i = 2, 3$. e is the neural identifier error.

The derivative of x_{2u} can be computed as follows

$$\dot{\hat{x}}_{2u} = g_{3v}^{-1} \left[\dot{\hat{T}}_{sm}\left(x_3, \hat{v}_w\right) + \tilde{x}_3 \dot{\hat{\xi}}_3 \right] + g_{3v}^{-1} \left(k_3 + \hat{\xi}_3\right) \left[T_{sm}\left(x_3, \hat{v}_w\right) - g_{3v} x_2 \right].$$

To approximate the derivative of T_{sm}, the robust exact differentiation technique proposed in [40] is used,

$$\begin{aligned} \dot{\hat{T}}_{sm} &= u_1 - \gamma \left| y - T_{sm} \right|^{1/2} \operatorname{sign} y - T_{sm}, \\ \dot{u}_1 &= -\sigma_T \operatorname{sign} y - T_{sm} \end{aligned}$$

with the auxiliary state $\dot{y} = \dot{\hat{T}}_{sm}$; where $\gamma, \sigma_T > 0$. It was proved that the difference between the $\dot{T}_{sm}$ and the $\dot{\hat{T}}_{sm}$ signals is bounded in finite time when the input signal presents noise. In the case when the signal has no noise, then, this difference is zero in finite time.

Now, let us propose the following Lyapunov candidate function

$$V_d = \frac{1}{2}\tilde{x}_3^2 + \frac{1}{2}z_1^2 + \frac{1}{2}z_2^2 + \frac{1}{4}e^4 + \frac{1}{2k_w^3} \sum_{j=1}^{N} \tilde{w_j^2}$$

where $z \triangleq [\tilde{x}_1,\ x_2 - x_{2u}]^T$ is the block of variables to be stabilized through the u signal directly.

The time derivative of V_d is

$$\begin{aligned}
\dot{V}_d &= \tilde{x}_3\dot{\tilde{x}}_3 + z_1\dot{z}_1 + z_2\dot{z}_2 + e^3\dot{e} + \frac{1}{k_w^3}\sum_{j=1}^{N}\dot{\hat{w}}_j\tilde{w}_j \\
&= \tilde{x}_3\left[T_{sm}(x_3, v_w) - g_{3v}x_2 + g_{3v}x_{2u} - g_{3v}x_{2u}\right] \\
&\quad + z_1\left[f_1 + g_1u\right] + z_2\left(f_2 + g_2u - \dot{x}_{2u}\right) + e^3\dot{e} \\
&\quad + \frac{1}{k_w^3}\sum_{j=1}^{N}\dot{\hat{w}}_j\tilde{w}_j \\
&= \tilde{x}_3\left[e_T - k_3\tilde{x}_3 - \hat{\xi}_3\tilde{x}_3 - g_{3v}z_2\right] + f_1z_1 \\
&\quad + z_2\left[f_2 - (\dot{\hat{x}}_{2u} + e_{2u})\right] + u(g_1z_1 + g_2z_2) \\
&\quad + e^3\dot{e} + \frac{1}{k_w^3}\sum_{j=1}^{N}\dot{\hat{w}}_j\tilde{w}_j
\end{aligned}$$

where the estimation errors are $e_T = T_{sm}(x_3, v_w) - T_{sm}(x_3, \hat{v}_w)$, and $e_{2u} = \dot{x}_{2u} - \dot{\hat{x}}_{2u}$. In order to stabilize the system, the control signal u can be chosen as follows

$$u_d \triangleq \frac{g_{3v}\tilde{x}_3z_2 - f_1z_1 - \left(f_2 - \dot{\hat{x}}_{2u}\right)z_2 - \kappa(z)}{g(z)} \tag{24}$$

where $\kappa(z) = k_1z_1^2 + \left(k_2 + \hat{\xi}_2\right)z_2^2$, $g(z) = g_1z_1 + g_2z_2$ and $u = u_d$. However, the denominator of the control law (24) can be zero or have a small value, resulting in infinite or big input control values. To avoid this problem, the gradient dynamics technique, recently proposed in [34], will be applied to the derived expression.

From (24), the following expression can be written

$$g(z)u_d - g_{3v}\tilde{x}_3z_2 + f_1z_1 + \left(f_2 - \dot{\hat{x}}_{2u}\right)z_2 + \kappa(z) = 0.$$

Following the gradient dynamics method, the following square-based nonnegative function is proposed:

$$\varphi \triangleq \frac{\mu^2}{2}$$

where $\mu \triangleq g(z)u - g_{3v}\tilde{x}_3z_2 + f_1z_1 + \left(f_2 - \dot{\hat{x}}_{2u}\right)z_2 + \kappa(z)$.

Now, the control dynamics can be designed as follows

$$\dot{u} \triangleq -k_u\frac{\partial\varphi}{\partial u} = -k_ug(z)\mu \tag{25}$$

where $k_u > 0$ is the convergence rate parameter.

Choosing the convergence rate as follows

$$k_u \geq \left|\frac{g - \dot{u}_d}{\frac{\partial\varphi}{\partial u}}\right| \tag{26}$$

then, the main result follows.

Theorem 1
Consider the system given by (4)–(5), the controller given by (25), and the identifier given by (18)–(21), satisfying Assumptions 1–5 and condition (26); then, uniform asymptotic stability of a small neighborhood of the origin of the variables $(\tilde{x}_3, z, e, \tilde{w}, \tilde{u})$ for the overall system is achieved.

Proof
Let us propose the following Lyapunov candidate function

$$V = V_d + \frac{1}{2}\tilde{u}^2$$

where $\tilde{u} \triangleq u - u_d$. Its time derivative is

$$\begin{aligned}
\dot{V} &= \dot{V}_d + \tilde{u}(\dot{u} - \dot{u}_d) \\
&= \tilde{x}_3\left[e_T - k_3\tilde{x}_3 - \hat{\xi}_3\tilde{x}_3 - g_{3v}z_2\right] + f_1 z_1 \\
&\quad + z_2\left[f_2 - (\dot{\hat{x}}_{2u} + e_{2u})\right] + (\tilde{u} + u_d)g(z) \\
&\quad + e^3\dot{e} + \frac{1}{k_w^3}\sum_{j=1}^{N}\dot{\hat{w}}_j\tilde{w}_j - \tilde{u}\left(k_u\frac{\partial\varphi}{\partial u} + \dot{u}_d\right) \\
&= \tilde{x}_3\left[e_T - k_3\tilde{x}_3 - \hat{\xi}_3\tilde{x}_3\right] + e_{2u}z_2 - \kappa(z) \\
&\quad + e^3\dot{e} + \frac{1}{k_w^3}\sum_{j=1}^{N}\dot{\hat{w}}_j\tilde{w}_j - \tilde{u}\left[k_u\frac{\partial\varphi}{\partial u} + \dot{u}_d - g(z)\right].
\end{aligned}$$

Using (23) and the fact that the signs of $\tilde{u}$ and $\frac{\partial\varphi}{\partial u}$ are equal due to the convex shape of φ, it yields

$$\begin{aligned}
\dot{V} \leqslant &-\kappa(z) - k_3\tilde{x}_3^2 - \hat{\xi}_3\tilde{x}_3^2 + e_T\tilde{x}_3 + e_{2u}z_2 \\
&- \hat{\lambda}_T e^4 + \lambda_T|e^3| - k_u|\tilde{u}|\left|\frac{\partial\varphi}{\partial u}\right| + \tilde{u}[g(z) - \dot{u}_d].
\end{aligned} \tag{27}$$

When the condition (26) is satisfied, and from the fact that the adaptive gains $\hat{\xi}_i$ and $\hat{\lambda}_T$ increase when the e error is not null; and that e_T, e_{2u} are bounded; and also because $e_T(e)$, $e_{2u}(e)$ are functions of the e error, then the following inequality holds

$$\lim_{t\to\infty}\hat{\xi}_2 z_2^2 + \hat{\xi}_3\tilde{x}_3^2 + \hat{\lambda}_T e^4 > \pi(\cdot) + \lambda_T|e^3| + \frac{1}{k_w^3}\sum_{j=1}^{N}\left|\dot{\hat{w}}_j\tilde{w}_j\right|$$

with $\pi(\cdot) = e_T\tilde{x}_3 + e_{2u}z_2$ and because the rest of the terms in (27) are negatives, then a small neighborhood of the origin of $(\tilde{x}_3, z, e, \tilde{w}, \tilde{u})$ is uniformly asymptotically stable.

Remark 6
Condition (26) can be satisfied when the right side of that equation is bounded. If the system is stable, then the only term that can make the equation unbounded is $\dot{u}_d$; and it happens when $g(z) \equiv 0$. There are three ways that this can happen:

1. when $g_1 z_1 \equiv -g_2 z_2$
2. when $x_1 \equiv 0$ and $x_2 \equiv 0$
3. when $z_1 \equiv 0$ and $z_2 \equiv 0$.

Because the first two conditions do not represent equilibrium points, as soon as they are reached, the system leaves them and reaches a different operation point. The third condition is the critical one, because it is precisely the desired equilibrium point—tracking errors and virtual control error equal to zero. This is the reason why the error origin cannot be uniformly asymptotically stable, but a small neighborhood of it. The system trajectories cannot reach this point —the error origin— but they will oscillate around it. At first glance, this would be like an inconvenience, but because the external input signal —the wind speed— is always varying, the third condition cannot be reached —permanently— in this kind of systems. □

6. COMPUTER SIMULATIONS

In order to show the performance of the controller and the identification algorithms proposed in this work, numerical simulations were made in the Simulink/Matlab environment. A wind speed profile with low-frequency and high-frequency components (Figure 5) was used for carrying out simulations on three adaptive schemes:

1. the GD-BBSC and the optimal mechanical torque point-based wind speed estimator proposed in this paper,
2. a PI controller and the I&I wind speed estimator,
3. the SPBC proposed in [2], and the I&I wind speed estimator.

The system parameters are the same in this last work and are shown in Table I. The nominal power of the considered wind turbine is 5 kVA.

The scaling factors in GD-BBSC were $s_1 = 1$, $s_2 = 10$, and $s_3 = 0.005$.

The initial conditions of the three controllers are shown in Table II. For the GD-BBSC, presetting (off-line training) of the weight vector was not necessary, and five nodes in the neural network were used to approximate T_{sm}. Special requirements in the initial conditions of the first two plant

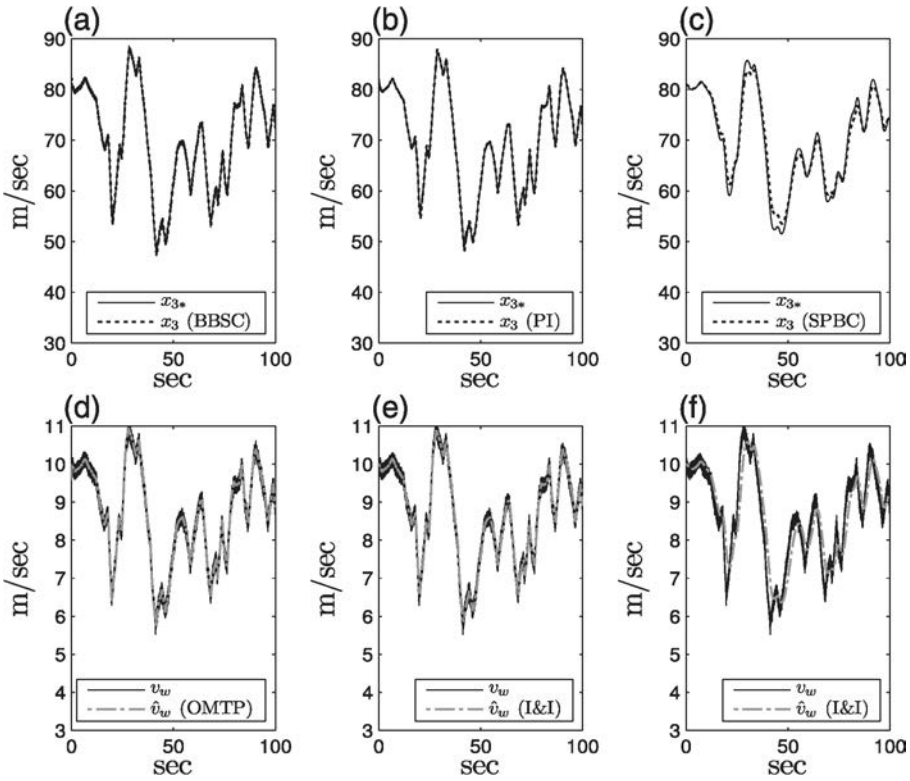

Figure 5. Reference tracking and wind speed estimation.

Table I. Wind turbine system parameters.

Parameter/element	Value
Nominal power	$S_n = 5000$ (VA)
Rotor inertia	$J = 7.856$ (kg m^2)
Blades radius	$r = 1.84$ (m)
Stator resistance	$R = 0.3676$ (Ω)
Stator inductance	$L = 0.00355$ (H)
Flux	$\phi = 0.2867$ (Wb)
Pole pairs	$P = 28$
Battery voltage	$v_b = 400$ (V)

Table II. Initial conditions.

GD-BBSC	PI controller	SPBC
Plant $x(0) = [0,\ 0,\ 0.62]^T$	$x(0) = [0,\ 0,\ 80]^T$	$x(0) = [1,\ 10,\ 81]^T$
Controller $u(0) = 0$ $\hat{\xi}_i(0) = 0$	$\zeta(0) = 0$	$x_d(0) = [1,\ 10,\ 81]^T$
Estimator $\hat{v}_w(0) = 10$ $\hat{x}_3(0) = 0.62$ $\hat{\lambda}_T(0) = 0$ $\hat{w}(0) = [0,\ 0,\ 0,\ 0,\ 0]^T$	$\hat{v}_w^I(0) = 10 - \gamma x_3(0)$	$\hat{v}_w^I(0) = 10 - \gamma x_3(0)$
Rotor speed reference $\hat{\tilde{x}}_{3*}(0) = 0$		

GD-BBSC, gradient dynamics-block-backstepping controller; SPBC, standard passivity-based controller.

states $[x_1,\ x_2]$, the adaptive gains $\hat{\xi}_i$, $\hat{\lambda}_T$, and the weight vector $\hat{w}$ of the neural network are not necessary as they can start far away from the optimal point. But the third state x_3, the identifier state $\hat{x}_3$, and the low-pass filter state $\hat{v}_w$ need initial conditions near to the optimal point to make the system work properly. With these initial conditions, the wind speed estimator and the controller are able to drive and keep the system in a neighborhood of its optimal power point, despite of fast and noisy wind speed signals as it can be appreciated in the next graphs. For the PI controller, the initial conditions on the first two plan states $[x_1,\ x_2]$ and the state of the integral part ζ can start in almost any condition. The third plant state x_3 and the estimator state $\hat{v}_w^I$ need to start relatively close to the optimal condition. This controller has the wider range of initial conditions for x_3. For the SPBC, this controller is not very sensitive to the initial conditions in the first two plant states $[x_1,\ x_2]$ and the controller states x_d, as they can start almost in any condition and the performance will be similar; however, the third plant state x_3 and the estimator state $\hat{v}_w^I$ need to start relatively close to the optimal condition. The initial condition of one of these states can be relaxed (start less closer to the optimal point), but not the initial conditions of both.

In order to test the reliability and robustness of the adaptive scheme proposed in this work, an additional simulation scenario was carried out for this scheme. This scenario consists in measurements with white noise in the i_d and i_q currents, that is, states $[x_1,\ x_2]$, and a linear variation in the stator resistance up to 20% in its nominal value.

In graphs (a), (b), and (c) of Figure 5, the third state reference x_{3*} and the third state x_3 for the GD-BBSC, the PI controller, and the SPBC, respectively, are shown. The GD-BBSC and the PI controller track in a precise way this reference. In contrast, the performance of the SPBC is not very good. This controller is not able to track medium and fast wind speed signals very well. Moreover, this controller not only cannot track fast wind speed signals, but with faster signals, the performance

degrades more. So the bandwidth of the input signal needs to be tuned carefully (with the adaptive gain of the I&I estimator), in order to get the optimal operation for this controller. However, even in its optimal operation, the deviations from the maximum power point are considerable as it can be seen in the next graphs. In graphs (d), (e), and (f) of the same figure, the wind speed profile and its estimations are shown. The low (shape) and high-frequency (boldness) components can be appreciated. Also, it can be appreciated in graph (d) that the performance of the estimation algorithm based in the optimal mechanical torque point, proposed in this paper, is good. In graph (e) we can observe the performance of the PI controller–I&I estimator; as it is well known, the performance of this estimator is good too. In graph (f), the performance of the SPBC–I&I estimator is shown; this time, the adaptive gain of the estimator was tuned conservatively in order to limit the bandwidth of the input signal in the SPBC.

Figure 6 shows the power coefficient function and the tip-speed ratio for the three schemes. Graphs (a), (b), and (c) show C_p for GD-BBSC, PI controller, and SPBC, respectively. The tip-speed ratio is shown in graphs (d), (e), and (f) for the same schemes. It can be noted that the deviations from their optimal points are small in the GD-BBSC and PI controllers. On the other hand, one can note that the deviations from their optimal points for the SPBC are big, especially in the sharpest parts of the wind speed profile. The deviations from the optimal point in λ are caused by the regulation of the third state x_3.

In graphs (a), (b), and (c) of Figure 7, the deviations from the maximum power point are shown for the three controllers. These comparative graphs reflect well the performance of the adaptive schemes. Small deviations can be noted in GD-BBSC, graph (a). The PI controller (graph (b)) presents deviations slightly bigger; whereas the biggest deviations can be appreciated in SPBC, graph (c). These deviations are caused by the deviations on the optimal λ, because the power

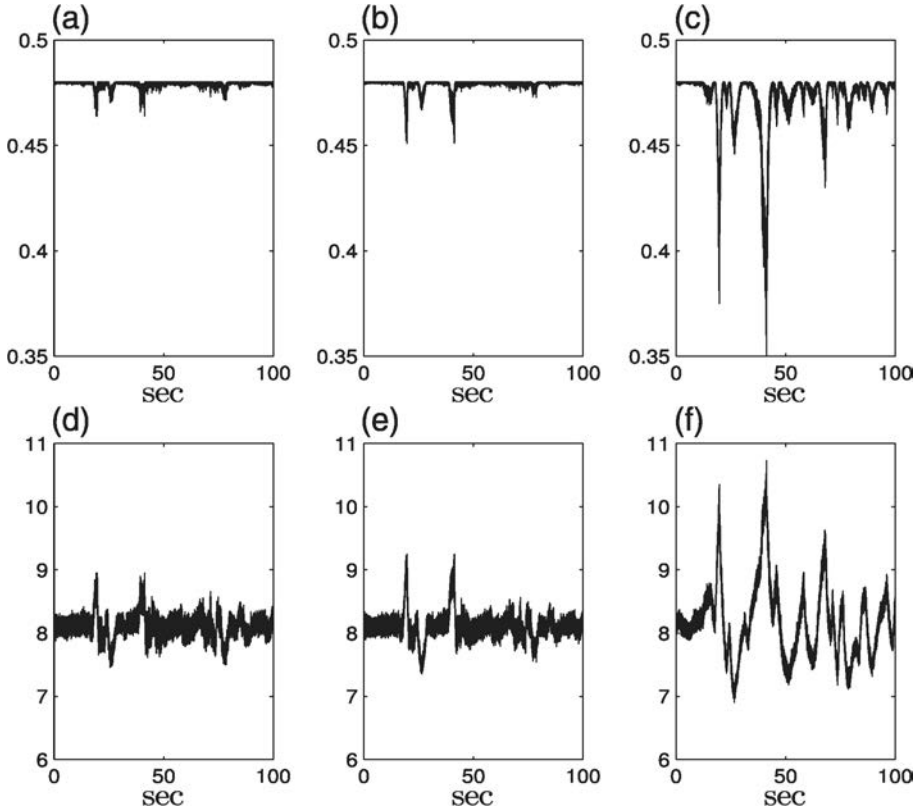

Figure 6. (a), (b), and (c) power coefficient C_p in gradient dynamics-block-backstepping controller, PI controller, and standard passivity-based controller, respectively. (d), (e), and (f) TSR λ in the same controllers.

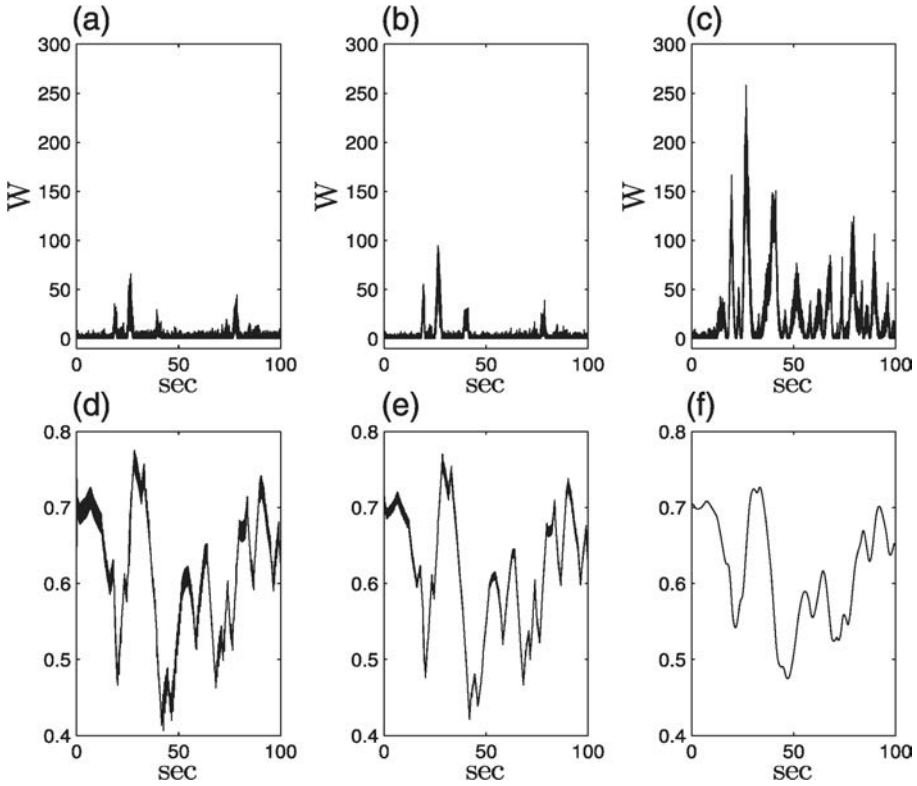

Figure 7. (a), (b), and (c) deviations from optimal power point in the gradient dynamics-block-backstepping controller, PI controller, and standard passivity-based controller, respectively. (d), (e), and (f) duty ratio D in the same controllers.

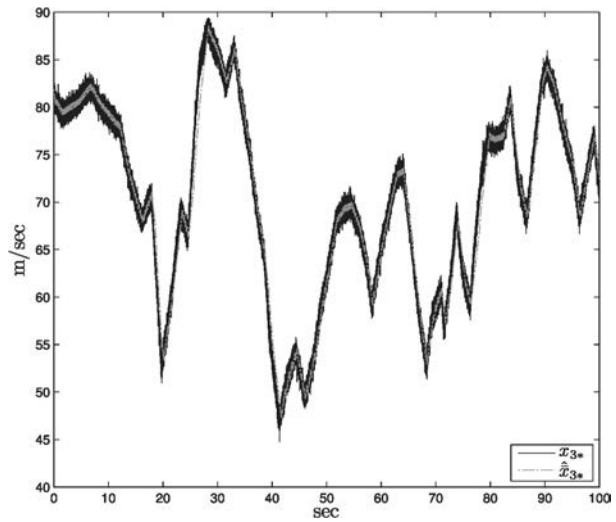

Figure 8. Optimal reference x_{3*} and estimated optimal reference $\hat{\hat{x}}_{3*}$.

coefficient is function of λ. Graphs (d), (e), and (f) show the duty ratio D of the DC–DC converter in the GD-BBSC, PI controller, and SPBC, respectively. All signals are in the [0, 1] interval.

Figure 8 shows the optimal reference x_{3*} for the third state and its estimation $\hat{\hat{x}}_{3*}$ given by the adaptive extremum-seeking algorithm. It can be seen that this estimation follows very well the true value of x_{3*}.

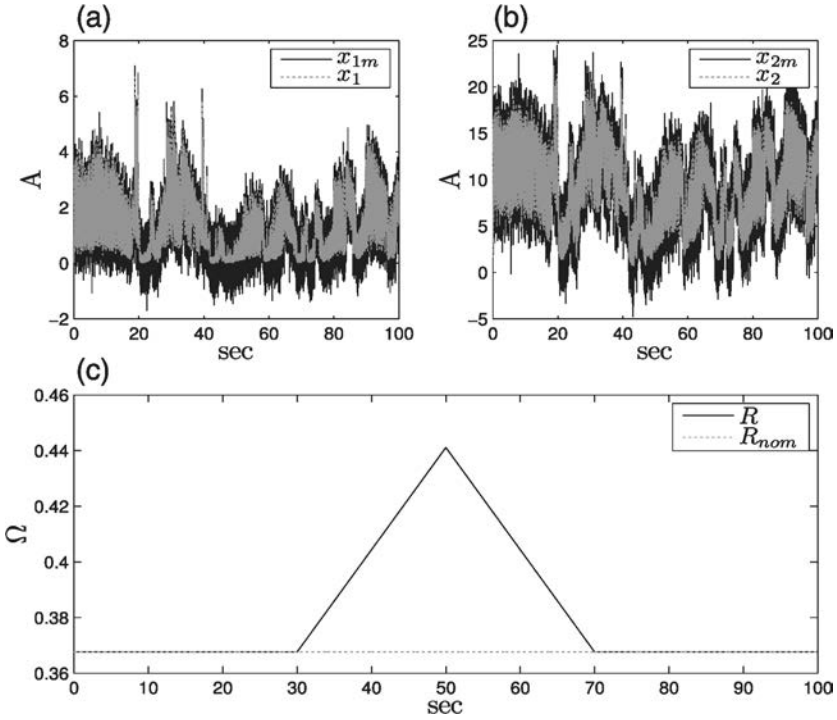

Figure 9. (a) and (b) measurements of the first two plant states x_1, x_2 with white noise: x_{1m}, x_{2m}. (c) linear variation in the nominal value of the stator resistance R.

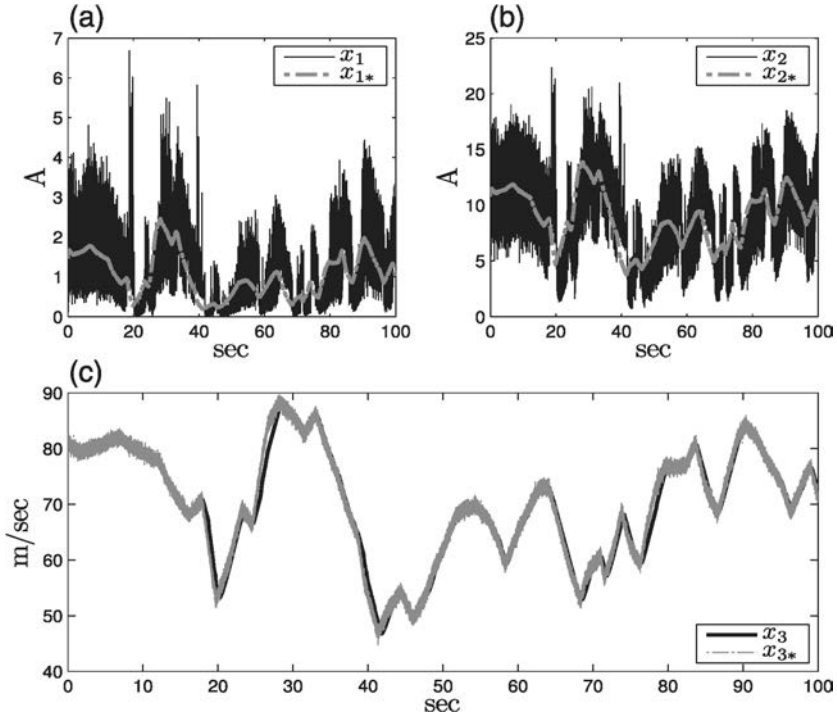

Figure 10. Reference tracking in the proposed adaptive scheme with noisy measurements and parameter uncertainties.

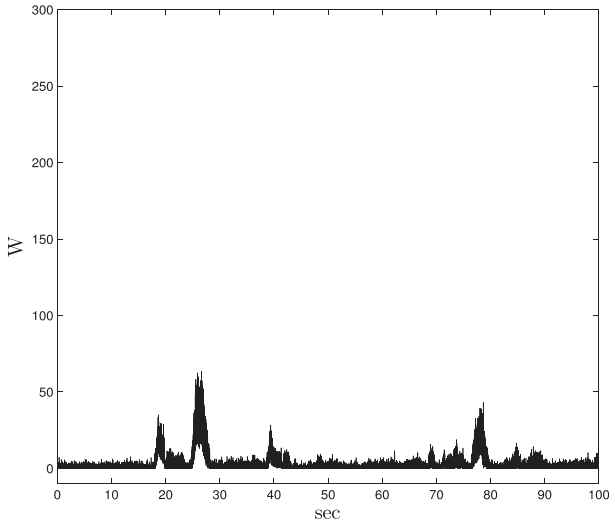

Figure 11. Deviations from optimal power point in the proposed adaptive scheme with noisy measurements and parameter uncertainties.

The robustness simulation scenario for the adaptive scheme proposed in this work is shown in Figures 9–11.

The measurements of the first two plant states (x_1, x_2) with white noise, x_{1m}, x_{2m}, are shown in graphs (a) and (b) of Figure 9. The linear variation in the stator resistance is shown in graph (c). This variation is up to 20% in its nominal value. The plant model includes the real values x_1, x_2, and R, whereas the controller and the identification algorithms use the measurements with white noise x_{1m}, x_{2m}, and the nominal value of the stator resistance R_{nom}.

Figure 10 shows the tracking of the three references in the proposed adaptive scheme, with noisy measurements and parameter uncertainties. It can be seen that despite the noisy measurements, the first two plant states follow the shape of their respective references. Also, it can be noted that the tracking of the rotor speed reference (x_{3*}) is good.

The deviations from the optimal power point in this simulation scenario are shown in Figure 11. It can be appreciated that these deviations remain small, even with the noisy measurements and the parameter uncertainties introduced in the system.

7. CONCLUSIONS

Wind speed and optimal reference estimation algorithms as well as GD-BBSC were presented in this work. The proposed adaptive scheme was able to follow very close the maximum power point of a stand-alone wind turbine system with a fast and noisy wind speed input signal.

The optimal reference estimation algorithm was derived using the sliding mode technique in an adaptive extremum-seeking framework. Uniform asymptotic stability of the error origin was proved using Lyapunov theories.

The procedure to calculate the wind speed signal was made using the mechanical torque equation evaluated at its optimal point. An artificial neural network with a dynamic nonlinear learning law of the weight vector was derived to estimate the mechanical torque signal. Uniform asymptotic stability of the error origin was proved using Lyapunov arguments.

A block-backstepping controller was derived to regulate the optimal equilibrium point. In order to avoid the singularities that can be present with the structure of this controller, the gradient dynamics technique was applied to this controller. Uniform asymptotic stability of a small neighborhood of the error origin was proved using Lyapunov theories for the overall system.

Computer simulations were carried out to show the performance of the proposed algorithms and to make comparisons with classical and passivity-based controllers. In addition, a numerical simulation

with noisy measurements and parameter uncertainties was made for the adaptive scheme proposed in this work. The simulated wind turbine was a stand-alone system with a nominal power of 5 kVA.

The numerical simulations showed the good performance of both estimation algorithms. The numerical simulation with noisy measurements and parameter uncertainties in the proposed adaptive scheme showed its reliability and robustness on these inconveniences.

Future work will be made to extend the range in the initial conditions in the third state of the system. Another future research direction is to extend this work to utility-scale wind turbine systems.

ACKNOWLEDGEMENTS

The work of F. Jaramillo-Lopez has been supported by CONACyT, Mexico, and the French Embassy in Mexico. This research has partially received support from the European Union Seventh Framework Programme [FP7/2007-2013] 257462 HYCON2 Network of excellence.

REFERENCES

1. Group 601 of Study Committee C4W. Modeling and dynamical behavior of wind generation as it relates to power system control and dynamic performance, *Final Report*, CIGRE, Jan 2007.
2. Mancilla-David F, Ortega R. Adaptive passivity-based control for maximum power extraction of stand-alone windmill systems. *Control Engineering Practice* 2012; **20**(2):173–181.
3. Johnson K, Pao L, Balas M, Fingersh L. Control of variable-speed wind turbines. *IEEE Control Systems Magazine* 2006; **26**(3):70–81.
4. Ortega R, Mancilla-David F, Jaramillo F. Globally convergent wind speed estimator for wind turbine systems. *International Journal of Adaptive Control and Signal Processing* 2013; **27**(5):413–425.
5. Chen S, Billings SA. Neural networks for nonlinear dynamic system modelling and identification. *International Journal of Control* 1992; **56**:319–346.
6. Chen S, Billings SA, Cowan CFN, Grant PM. Practical identification of narmax models using radial basis functions. *International Journal of Control* 1990; **52**:1327–1350.
7. Kenne G, Ahmed-Ali T, Lamnabhi-Lagarrigue F, Nkwawo H. Nonlinear systems parameters estimation using radial basis function network. *Control Engineering Practice* 2006; **14**(7):819–832.
8. Ahmed-Ali T, Kenne G, Lamnabhi-Lagarrigue F. Identification of nonlinear systems with time-varying parameters using a sliding-neural network observer. *Neurocomputing* 2009; **72**(7-9):1611–1620.
9. Qiao W, Gong X, Qu L. Output maximization control for DFIG wind turbines without using wind and shaft speed measurements. *Proceedings of IEEE Energy Conversion Congress and Exposition* 2009:404–410.
10. Pucci M, Vitale G. Growing neural gas (GNG)-based maximum power point tracking for high-performance wind generator with an induction machine. *IEEE Transactions on Industry Applications* 2011; **47**(2):861–872.
11. Li H, Shi K, McLaren P. Neural network based sensorless maximum wind energy capture with compensated power coefficient. *IEEE Transactions on Industry Applications* 2005; **41**(6):1548–1556.
12. Qiao W, Zhou W, Aller J, Harley R. Wind speed estimation based sensorless output maximization control for a wind turbine driving a DFIG. *IEEE Transactions on Power Electronics* 2008; **23**(3):1156–1169.
13. Boukhezzar B, Siguerdidjane H, Hand M. Nonlinear control of variable-speed wind turbines for generator torque limiting and power optimization. *ASME Journal of Solar Energy Engineering* 2006; **128**(4):516–530.
14. Guay M, Dochain D, Perrier M. Adaptive extremum seeking control of continuous stirred tank bioreactors with unknown growth kinetics. *Automatica* 2004; **40**(5):881–888.
15. Zhang C, Siranosian A, Krstic M. Extremum seeking for moderately unstable systems and for autonomous vehicle target tracking without position measurements. *Automatica* 2007; **43**:1832–1839.
16. Peterson K, Stefanopoulou A. Extremum seeking control for soft landing of an electromechanical valve actuator. *Automatica* 2004; **40**:1063–1069.
17. Ren B, Frihauf P, Rafac R, Krstic M. Laser pulse shaping via extremum seeking. *Control Engineering Practice* 2012; **20**:674–683.
18. Guay M, Zhang T. Adaptive extremum seeking control of nonlinear dynamic systems with parametric uncertainties. *Automatica* 2003; **39**:1283–1293.
19. Moase W, Manzie C, Brear M. Newton-like extremum-seeking part i: theory. *Joint 48th IEEE Conference on Decision and Control and 28th Chinese Control Conference*, Shanghai, P.R. China, 2009; 3839–3844.
20. Abdullah M, Yatim A, Tan C, Saidur R. Review of maximum power point tracking algorithms for wind energy systems. *Renewable and Sustainable Energy Reviews* 2012; **16**:3220–3227.
21. Kot R, Rolak M, Malinowski M. Comparison of maximum peak power tracking algorithms for a small wind turbine. *Mathematics and Computers in Simulation* 2013; **91**:29–40.
22. Gonzalez L, Figueres E, Garcera G, Carranza O. Maximum-power-point tracking with reduced mechanical stress applied to wind-energy-conversion-systems. *Applied Energy* 2010; **87**:2304–2312.
23. Krstic M, Wang H. Stability of extremum seeking feedback for general nonlinear dynamic systems. *Automatica* 2000; **36**:595–601.

24. Ko H, Yoon G, Kyung N, Hong W. Modeling and control of DFIG-based variable-speed wind-turbine. *Electric Power Systems Research* 2008; **78**:1841–1849.
25. Boukhezzar B, Lupu L, Siguerdidjane H, Hand M. Multivariable control strategy for variable speed, variable pitch wind turbines. *Renewable Energy* 2007; **32**:1273–1287.
26. Li S, Haskew T, Xu L. Conventional and novel control designs for direct driven PMSG wind turbines. *Electric Conventional Power Systems Research* 2010; **80**:328–338.
27. Kim H, Kim S, Ko H. Modeling and control of PMSG-based variable-speed wind turbine. *Electric Power Systems Research* 2010; **80**:46–52.
28. Corradini M, Ippoliti G, Orlando G. Fully sensorless robust control of variable-speed wind turbines for efficiency maximization. *Automatica* 2013; **49**:3023–3031.
29. El Magri A, Giri F, Besancon G, El Fadili A, Dugard L, Chaoui F. Sensorless adaptive output feedback control of wind energy systems with PMS generators. *Control Engineering Practice* 2013; **21**:530–543.
30. Odgaard P, Stoustrup J, Kinnaert M. Fault-tolerant control of wind turbines: a benchmark model. *IEEE Transactions on Control Systems Technology* 2013; **21**(4):1168–1182.
31. Odgaard P, Johnson K. Wind turbine fault detection and fault tolerant control - an enhanced benchmark challenge. *Proc. of the 2013 American Control Conference*, Washington, DC, USA, 2013; 4453–4458.
32. Johnson K, Fleming P. Development, implementation, and testing of fault detection strategies on the national wind technology center's controls advanced research turbines. *Mechatronics* 2011; **21**:728–736.
33. Galvez M. Sensor fault diagnosis for wind-driven doubly-fed induction generators. *PhD Thesis*, Université Libre de Bruxelles, Bruxelles.
34. Zhang Y, Yu X, Yin Y, Xiao L, Fan Z. Using GD to conquer the singularity problem of conventional controller for output tracking of nonlinear system of a class. *Physics Letters A* 2013; **377**:1611–1614.
35. Slootweg J, de Haan S, Polinder H, Kling W. General model for representing variable speed wind turbines in power system dynamics simulations. *IEEE Transactions on Power Systems* 2003; **18**(1):144–151.
36. MathWorks. *Simpowersystems blockset user's guide*, 2011. Available from: http://www.mathworks.com/ [Accessed on July 2014].
37. Phankong N, Manmai S, Bhumkittipich K, Nakawiwat P. Modeling of grid-connected with permanent magnet synchronous generator (PMSG) using voltage vector control. *Energy Procedia* 2013; **34**:262–272.
38. Ackermann T. *Wind Power in Power Systems*. John Wiley & Sons, Ltd: UK, 2005.
39. Khalil H. *Nonlinear Systems* (3rd edn). Prentice-Hall: New York, 1996.
40. Levant A. Robust exact differentiation via sliding mode technique. *Automatica* 1998; **34**(3):379–384.